18F-Fluoro-L-Thymidine and 11C-Methylmethionine as Markers of Increased Transport and Proliferation in Brain Tumors

Andreas H. Jacobs, MD[1–3]; Anne Thomas, MD[1,2]; Lutz W. Kracht, MD[1]; Huongfeng Li, PhD[1]; Claus Dittmar, PhD[1]; Guido Garlip, MD[1]; Norbert Galldiks, MD[1]; Johannes C. Klein, MD[1]; Jan Sobesky, MD[1,2]; Rüdiger Hilker, MD[1,2]; Stefan Vollmar, PhD[1,2]; Karl Herholz, MD[1,2] Klaus Wienhard, PhD[1]; and Wolf-Dieter Heiss, MD[1–3]

[1]Max Planck Institute for Neurological Research, Cologne, Germany; [2]Department of Neurology, University of Cologne, Cologne, Germany; and [3]Center for Molecular Medicine, University of Cologne, Cologne, Germany

Because of the high glucose metabolism in normal brain tissue ^{18}F-FDG is not the ideal tracer for the detection of gliomas. Methyl-^{11}C-L-methionine (^{11}C-MET) is better suited for imaging the extent of gliomas, because it is transported specifically into tumors but only insignificantly into normal brain. 3′-Deoxy-3′-^{18}F-fluorothymidine (^{18}F-FLT) has been introduced as a proliferation marker in a variety of neoplasias and has promising potential for the detection of brain tumors, because its uptake in normal brain is low. Additionally, the longer half-life might permit differentiation between transport and intracellular phosphorylation. **Methods:** PET of ^{18}F-FLT and ^{11}C-MET was performed on 23 patients (age range, 20–70 y) with histologically verified gliomas of different grades. On all patients, conventional MRI was performed, and 16 patients additionally underwent contrast-enhanced imaging. Images were coregistered, and the volumes of abnormality were defined for PET and MRI. Uptake ratios and standardized uptake values (SUVs) of various tumors and regions were assessed by region-of-interest analysis. Kinetic modeling was performed on 14 patients for regional time–activity curves of ^{18}F-FLT from tumorous and normal brain tissue. **Results:** Sensitivity for the detection of tumors was lower for ^{18}F-FLT than for ^{11}C-MET (78.3% vs. 91.3%), especially for low-grade astrocytomas. Tumor volumes detected by ^{18}F-FLT and ^{11}C-MET were larger than tumor regions displaying gadolinium enhancement ($P < 0.01$). Uptake ratios of ^{18}F-FLT were higher than uptake ratios of ^{11}C-MET ($P < 0.01$). Uptake ratios of ^{18}F-FLT were higher in glioblastomas than in astrocytomas ($P < 0.01$). Absolute radiotracer uptake of ^{18}F-FLT was low and significantly lower than that of ^{11}C-MET (SUV, 1.3 ± 0.7 vs. 3.1 ± 1.0; $P < 0.01$). Some tumor regions were detected only by either ^{18}F-FLT (7 patients) or ^{11}C-MET (13 patients). Kinetic modeling revealed that ^{18}F-FLT uptake in tumor tissue seems to be predominantly due to elevated transport and net influx. However, a moderate correlation was found between uptake ratio and phosphorylation rate k_3 ($r = 0.65$ and $P = 0.01$ for grade II–IV gliomas; $r = 0.76$ and $P < 0.01$ for grade III–IV tumors). **Conclusion:** ^{18}F-FLT is a promising tracer for the detection and characterization of primary central nervous system tumors and might help to differentiate between low- and high-grade gliomas. ^{18}F-FLT uptake is mainly due to increased transport, but irreversible incorporation by phosphorylation might also contribute. In some tumors and tumor areas, ^{18}F-FLT uptake is not related to ^{11}C-MET uptake. In view of the high sensitivity and specificity of ^{11}C-MET PET for imaging of gliomas, it cannot be excluded that ^{18}F-FLT PET was false positive in these areas. However, the discrepancies observed for the various imaging modalities (^{18}F-FLT and ^{11}C-MET PET as well as gadolinium-enhanced MRI) yield complementary information on the activity and the extent of gliomas and might improve early evaluation of treatment effects, especially in patients with high-grade gliomas. Further studies are needed, including coregistered histology and kinetic analysis in patients undergoing chemotherapy.

Key Words: brain tumor; PET; ^{18}F-FLT; ^{11}C-MET

J Nucl Med 2005; 46:1948–1958

Methyl-^{11}C-L-methionine (^{11}C-MET) and ^{18}F-FDG are well-established markers in brain tumor diagnosis. Although the potential of ^{18}F-FDG in the diagnosis of cortical gliomas is limited because of the hypo- or isometabolism of some tumors, ^{11}C-MET has been shown to possess high specificity in tumor detection, tumor delineation, and differentiation of benign from malignant lesions (*1*). ^{11}C-MET uptake, which seems to be caused by increased carrier-mediated transport rather than elevated protein synthesis, correlates with cell proliferation, in vitro Ki-67 expression, and proliferating cell nuclear antigen expression (*2–4*) as well as with microvessel density (*5*). Unfortunately, the short half-life of ^{11}C (20 min) and the rapid catabolism of methionine in vivo limits kinetic modeling for this tracer.

Recently, Shields et al. have developed the new PET tracer, 3′-deoxy-3′-^{18}F-fluorothymidine (^{18}F-FLT), which allows for noninvasive assessment of tumor proliferation (*6*). In contrast to ^{18}F-FDG and ^{11}C-MET, which provide only an indirect measure of proliferation status, ^{18}F-FLT allows the direct measurement of cellular thymidine kinase

activity, which is proportional to the proliferative activity of the tumor, and early assessment of response to therapy. After phosphorylation by cellular thymidine kinase 1 (TK_1), ^{18}F-FLT nucleotides are trapped within the cell (7). Although in normal cells TK_1 activity is increased by about 10-fold only during the DNA synthetic phase (8), in malignant cells the increase in TK_1 activity is higher and permanent (9,10).

^{18}F-FLT uptake has already been demonstrated in a variety of tumors such as lung cancer, colorectal carcinoma, malignant melanoma, and non-Hodgkin's lymphoma (11–14). Several studies detected a strong correlation between the standardized uptake value (SUV) of ^{18}F-FLT and the proliferative status in corresponding tumor samples (11,14). In cell culture experiments, ^{18}F-FLT uptake correlated well with percentage of cells in S-phase and TK_1 activity (15). Because uptake of ^{18}F-FLT is low in intact brain tissue, ^{18}F-FLT provides a low-background cerebral image and thus is considered to be an attractive PET tracer for the imaging of brain tumors.

The purpose of this prospective study was to clarify the role of ^{18}F-FLT in the diagnosis of primary central nervous system tumors. We therefore compared the newly developed ^{18}F-FLT PET with the routinely used ^{11}C-MET PET and contrast-enhanced MRI to determine DNA metabolism and amino acid uptake as well as the integrity of the blood–brain barrier in patients with gliomas.

MATERIALS AND METHODS

Patients

Twenty-three patients with primary central nervous system tumors (11 men and 12 women; mean age, 47.1 ± 14.6 y; range, 20–70 y) were included in this prospective study after giving their informed consent. Diagnoses had been confirmed histologically according to World Health Organization (WHO) criteria in all patients before or after the PET examination. Tumor types and grades were distributed as follows: WHO grade I astrocytoma (n = 1); WHO grade II astrocytoma (n = 6); WHO grade II oligoastrocytoma (n = 2); WHO grade III astrocytoma (n = 4); WHO grade III oligodendroglioma (n = 1); WHO grade III oligoastrocytoma (n = 1); anaplastic ganglioglioma (n = 1); WHO grade IV glioblastoma (n = 6); and WHO grade IV medulloblastoma (n = 1). Because patients partly had received different therapy schemes before being included in the study, the WHO groups were divided into a treated subgroup (n = 15) and an untreated subgroup (n = 8). Individual clinical data are summarized in Table 1.

PET Studies

Data Acquisition. PET imaging devices were an ECAT EXACT (CTI/Siemens; in-plane full width at half maximum, 6 mm; slice thickness, 3.375 mm; axial field of view, 162 mm) and an ECAT

TABLE 1
Characteristics of 22 Patients with Glioma and 1 Patient with Medulloblastoma

Patient no.	Age (y)	Sex	Tumor type and WHO grade	Location	Side	ND/REC	Therapy before study entry		
							Surgery	Radiation (Gy)	Chemotherapy
1	33	F	Astrocytoma II	Frontal	R	REC	1	54	—
2	59	F	Glioblastoma IV	Temporal	L	REC	2	60	TMZ
3	51	F	Astrocytoma II	Precentral	R	REC	1	—	—
4	49	F	Glioblastoma IV	Temporal	L	REC	1	60	TMZ 5C
5	70	M	Glioblastoma IV	Frontoparietal	R	ND	—	—	—
6	50	F	Astrocytoma II	Frontotemporal	L	REC	1	—	—
7	64	M	Glioblastoma IV	Frontal	R	ND	—	—	—
8	67	M	Glioblastoma IV	Parietooccipital	L	ND	—	—	—
9	39	F	Astrocytoma III	Brainstem, thalamus	L	REC	—	60	TMZ 4C, PCV 5C
10	35	F	Glioblastoma IV	Temporal	R	REC	2	60	TMZ
11	20	M	Medulloblastoma IV	Cerebellar	R	REC	2	3×	HIT-91, 97, 3×
12	38	M	Astrocytoma III	Parietooccipital	L	REC	1	60	PCV 2C
13	57	F	Oligoastrocytoma II	Thalamus	R and L	REC	3	60	—
14	58	F	Ganglioglioma III	Temporoparietal	L	REC	—	—	PCV 1C
15	34	M	Astrocytoma II	Precentral	L	ND	—	—	—
16	38	M	Astrocytoma II	Temporoparietal	L	REC	1	—	TMZ 9C
17	26	F	Astrocytoma I	Occipital	R	ND	—	—	—
18	47	F	Oligoastrocytoma III	Parietal	L	REC	1	60	TMZ
19	33	M	Astrocytoma III	Frontoparietal	R	REC	1	—	PCV 4C
20	55	M	Oligoastrocytoma II	Temporoparietooccipital	L	REC	1	—	—
21	60	F	Oligodendroglioma III	Parietal	L	ND	—	—	—
22	31	M	Astrocytoma II	Temporoparietal	L	ND	—	—	—
23	69	M	Astrocytoma II	Occipital	R	ND	—	—	—

ND = newly diagnosed; REC = recurrent; TMZ = temozolomide; PCV = procarbazine, lomustine, and vincristine; HIT = randomized, prospective, multicenter trial in order to improve the survival of children with medulloblastoma by using postoperative neoadjuvant chemotherapy before radiation therapy as opposed to maintenance chemotherapy after immediate postoperative radiotherapy.

EXACT HR (CTI/Siemens; in-plane full width at half maximum, 3.6 mm; slice thickness, 3.125 mm; axial field of view, 150 mm). For attenuation correction, 10-min transmission scans with 3 rotating ^{68}Ga/^{68}Ge sources were obtained before tracer application.

All patients were examined using ^{11}C-MET and ^{18}F-FLT synthesized according to the method of Machulla et al. (16) and Wodarski et al. (17). The radiolabeling yield of ^{18}F-FLT was 6.3% ± 1.3%, and the radiochemical purity of ^{18}F-FLT was 98%.

After injection of 677.1 ± 148.0 MBq (range, 222–720 MBq) of ^{11}C-MET, tracer accumulation was recorded over 60 min in 47 transaxial slices of the entire brain as described elsewhere (5).

The mean dose of ^{18}F-FLT was 321.9 ± 85.1 MBq (range, 111–370 MBq). For kinetic analysis of ^{18}F-FLT, arterialized blood samples were obtained from 14 patients using an intravenous catheter separate from that used for tracer injection. The hand of the patient was kept in a 40°C water bath from at least 10 min before the PET examination until the end of the examination to ensure sufficient arterial-venous shunting. The oxygenation status of a blood sample was measured before the start of the PET examination to ensure that oxygenation was greater than 85%. ^{18}F-FLT PET images were acquired as a 90-min dynamic set comprising the following frame durations: 6 × 10 s, 3 × 20 s, 2 × 30 s, 2 × 60 s, 2 × 150 s, and 16 × 300 s.

To allow for coregistration of metabolic and anatomic data, digitally delivered T1- and T2-weighted MRI was performed on a 1.5-T system (Gyroscan Intera; Philips Medical Systems) for all patients. Contrast-enhanced T1-weighted MRI was performed on 16 of the 23 patients. Multitracer PET and MRI scans were completed within 6.3 ± 3.0 d (range, 2–13 d).

Data Analysis. For 2 patients, the results of both ^{11}C-MET PET and ^{18}F-FLT PET were false negative, and these data were thus exempted from further analysis. Tumor volumes were defined in the remaining 21 and 14 patients for PET and contrast-enhanced MRI, respectively, using the 3D-Tool, which was developed in-house. The threshold for increased ^{11}C-MET uptake was set to 1.3 (18), the threshold for increased ^{18}F-FLT uptake was set to 2.0, and the threshold for positive contrast enhancement on MRI was determined by varying the lower value to match the area of positive enhancement on individual MRI scans. To all 3 imaging modalities, a component analyses was applied to extract areas of positive enhancement or tracer uptake outside the brain, such as high ^{11}C-MET uptake in lacrimal or pituitary glands and high ^{18}F-FLT uptake in bone and venous sinuses.

A region-of-interest (ROI) approach was used to compare tracer uptake in ^{11}C-MET and ^{18}F-FLT PET. To determine maximal tracer uptake, a circular ROI 8 mm in diameter was placed on the areas of highest ^{11}C-MET and ^{18}F-FLT uptake. For reference, a commensurate ROI was placed on the corresponding contralateral region or, if impossible because of the tumor location, on intact brain regions. Uptake ratios and SUVs were calculated as described elsewhere (5,19).

For further differentiation of ^{11}C-MET, ^{18}F-FLT, and gadolinium-diethylenetriaminepentaacetic acid (DTPA) uptake, detailed, irregularly shaped ROIs were placed on coregistered PET and available MRI scans where increased uptake of ^{18}F-FLT alone, ^{11}C-MET alone, gadolinium-DTPA alone, or a combination of any of these was observed. A circular ROI was placed on the nasal mucosa, being a rapidly dividing tissue with presumed high TK_1 activity. Because of the variation in ROI size, reference ROIs

were placed on intact gray and white matter to calculate the uptake ratios.

For kinetic analysis of ^{18}F-FLT, time–activity curves were generated from circular regions placed over the tumor region with maximum tracer uptake. Because of low counts in intact brain tissue, reference ROIs were enlarged to the whole contralateral hemisphere to improve kinetic fitting. Time–activity curves obtained from 3 consecutive slices of the dynamic image set were analyzed by the PMOD biomedical image quantification and kinetic modeling software (PMOD Technologies Ltd.).

A three-compartment (4 rate constants) model was used to describe tracer kinetics. In this model, K1 and k2 are rate constants describing tracer influx and efflux from plasma to tissue, respectively. The metabolic rate constant k3 describes the phosphorylation rate of ^{18}F-FLT by TK_1. The dephosphorylation constant k4 was either set to zero (20,21) or also included into the fitting procedure. The net influx constant Ki of ^{18}F-FLT into the respective regions was calculated as follows: Ki = K1 × k3/(k2 + k3). Additionally, blood volume was assessed in both tumor and reference regions.

Statistical Analysis

The Wilcoxon signed rank test, the Mann–Whitney rank sum test, and Spearman correlation analysis were used to assess the significance of any differences. Differences were considered statistically significant when P was <0.05.

RESULTS

Sensitivity of ^{18}F-FLT PET in Detecting Gliomas Is Lower Than Sensitivity of ^{11}C-MET PET

Of the 23 tumors studied, 21 (91.3%) were imaged by ^{11}C-MET PET and 18 (78.3%) by ^{18}F-FLT PET. Tumors that were false negative on ^{11}C-MET PET ($n = 2$) also were false negative on ^{18}F-FLT PET; thus, no tumors were detected by ^{18}F-FLT PET only. Of the tumors that were false negative on ^{18}F-FLT PET ($n = 5$), 1 exhibited slight contrast enhancement by MRI, 3 did not show contrast enhancement, and for 1 the diagnosis was made by ^{11}C-MET PET, without an MRI examination (Table 2). Both tracers failed to detect WHO grade II astrocytomas; ^{18}F-FLT PET additionally was false negative in 1 case of WHO grade III oligodendroglioma. All tumors showing positive contrast enhancement on MRI ($n = 13$) were depicted by ^{11}C-MET PET, 1 of these patients had false-negative ^{18}F-FLT uptake.

These data indicate that, in this study, ^{18}F-FLT PET was less sensitive than ^{11}C-MET PET in detecting primary central nervous system tumors, especially WHO grade II astrocytomas.

Figure 1 gives 2 examples of increased ^{18}F-FLT uptake in regions of increased gadolinium uptake, with additional information on the true extent of the tumor given by ^{11}C-MET PET. Figure 2 gives an example of a false-negative result on ^{18}F-FLT PET. Figures 3 and 4 give examples of patients for whom complementary information on the activity and extent of the tumor could be obtained by ^{18}F-FLT PET.

TABLE 2
Results for 23 Patients Undergoing PET and MRI

Patient no.	Tumor volume (cm³) as determined by . . .			Normalized tumor volume			Radiotracer uptake ratio*		SUV	
	^{18}F-FLT	^{11}C-MET	MRI-Gd	FLT/Gd	MET/Gd	MET/FLT	^{18}F-FLT	^{11}C-MET	^{18}F-FLT	^{11}C-MET
1	5.0	7.6	—	—	—	1.5	2.4	1.6	1.1	2.5
2	27.4	27.5	6.8	4.0	4.0	1.0	7.9	3.3	1.7	3.6
3	7.9	18.5	—	—	—	2.3	4.4	2.7	1.0	3.1
4	91.2	52.7	20.5	4.5	2.6	0.6	9.3	2.7	2.7	5.4
5	46.6	46.0	—	—	—	1.0	7.0	3.5	1.3	3.3
6	0	5.7	1.2	0	4.9	—	(1.0)	1.6	(0.2)	1.9
7	60.4	51.8	37.8	1.6	1.4	0.9	6.4	2.6	1.2	3.4
8	42.7	66.3	—	—	—	1.6	6.9	2.7	1.5	3.3
9	7.7	35.3	2.6	3.0	13.7	4.6	3.8	2.4	1.4	2.8
10	8.3	1.0	3.3	2.5	0.3	0.1	3.7	1.2	0.7	1.6
11	5.5	3.7	1.6	3.3	2.2	0.7	3.3	1.4	1.8	4.2
12	8.9	20.6	—	—	—	2.3	2.1	1.7	0.5	2.4
13	3.9	42.6	0.1	29.9	327.8	11.0	1.3	2.3	0.5	3.2
14	40.0	35.6	14.4	2.8	2.5	0.9	13.0	4.7	3.0	3.9
15	0	0	0	—	—	—	(1.0)	(1.0)	(0.2)	(1.0)
16	0	18.8	—	—	—	—	(1.0)	2.0	(0.4)	2.6
17	7.7	14.3	5.5	1.4	2.6	1.9	3.9	2.3	1.4	4.0
18	0.4	20.6	1.1	0.4	19.4	46.8	2.0	1.3	0.8	2.6
19	17.4	24.7	6.8	2.6	3.6	1.4	3.5	1.9	0.6	2.0
20	1.7	28.0	—	—	—	16.3	2.0	2.7	0.5	3.1
21	0	14.6	0	—	—	—	(1.0)	1.8	(0.3)	4.3
22	0	0	0	—	—	—	(1.0)	(1.0)	(0.2)	(1.0)
23	14.7	34.4	10.7	1.4	3.2	2.3	4.7	2.1	1.3	1.3
Mean	18.9	27.1	8.0	4.4	29.9	5.4	4.9	2.3	1.3	3.1
SD	24.2	17.6	10.4	7.8	89.7	11.1	3.0	0.8	0.7	1.0

*Calculated by dividing circular ROIs placed over tumor tissue by circular ROIs placed over intact brain. Uptake ratios of false-negative tumors in either PET examination were set to 1.
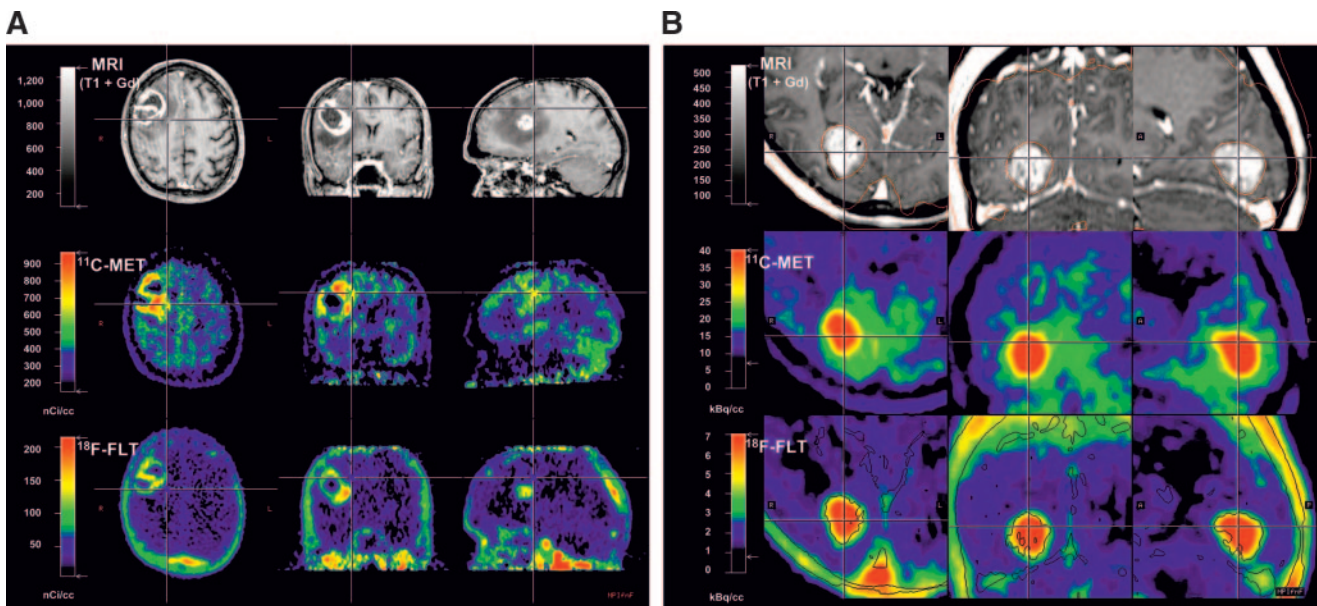
FIGURE 1. Two patients with highly intense ^{18}F-FLT accumulation that was found mainly in areas of breakdown of blood–brain barrier as depicted by gadolinium-enhanced MRI. A 64-y-old man with newly diagnosed glioblastoma (A) and 26-y-old woman with newly diagnosed WHO grade I astrocytoma (B). In both patients, ^{11}C-MET PET is suggestive of a larger extent of tumor as depicted by gadolinium MRI.
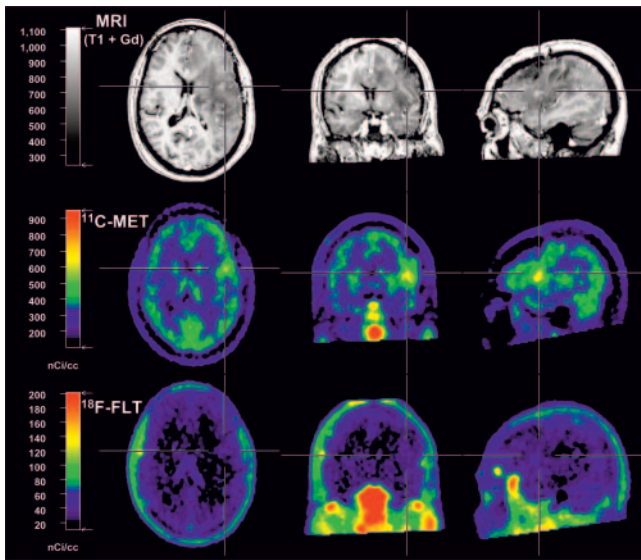
FIGURE 2. False-negative findings on ^{18}F-FLT PET in 50-y-old woman with WHO grade II astrocytoma that had been resected at primary diagnosis. At a regular follow-up, MRI depicted signal changes within large parts of left hemisphere with only minor gadolinium enhancement (volume, 1.2 cm³) and area of mildly increased ^{11}C-MET uptake (volume, 5.7 cm³; factor, 1.6). Mucosa and cranial bone marrow show intense ^{18}F-FLT uptake, whereas ^{18}F-FLT background in normal brain is low.

Tumor Volumes Defined by ^{18}F-FLT PET and ^{11}C-MET PET Are Larger Than Blood–Brain Barrier Breakdown Detected by Gadolinium-Enhanced MRI

The mean tumor volumes as measured with the 3D-Tool were 27.1 ± 17.6 cm³ in ^{11}C-MET PET, 18.9 ± 24.2 cm³ in ^{18}F-FLT PET, and 8.0 ± 10.4 cm³ in gadolinium-positive MRI. Individual tumor volumes are depicted in Table 2. In 11 of 16 patients, tumor volumes as measured by ^{18}F-FLT PET, ranging from a factor of 1.4 to 29.9 (mean, 4.4), were greater than tumor volumes as measured by gadolinium-enhanced MRI. Examples are given in Figures 3 and 4. In 12 of 16 patients, tumor volumes as measured by ^{11}C-MET PET, ranging from a factor of 1.4 to 327.8 (mean, 29.9), were greater than tumor volumes as measured by gadolinium-enhanced MRI (Table 2). In only 1 patient each was the tumor volume as measured by ^{11}C-MET or ^{18}F-FLT PET smaller than the tumor volume as measured by gadolinium-enhanced MRI. Normalized tumor volumes (FLT/gadolinium and MET/gadolinium) are also depicted in Table 2. As expected, tumor volumes on gadolinium-positive MRI were significantly smaller than those on ^{11}C-MET and ^{18}F-FLT PET (Wilcoxon, $P < 0.01$). There was a positive correlation between tumor volumes as measured by PET and tumor volumes as measured by MRI (Wilcoxon, $P < 0.01$). The relationship between tumor volumes as measured by ^{11}C-MET PET and ^{18}F-FLT PET in comparison with gadolinium-enhanced MRI is depicted in Figure 5.
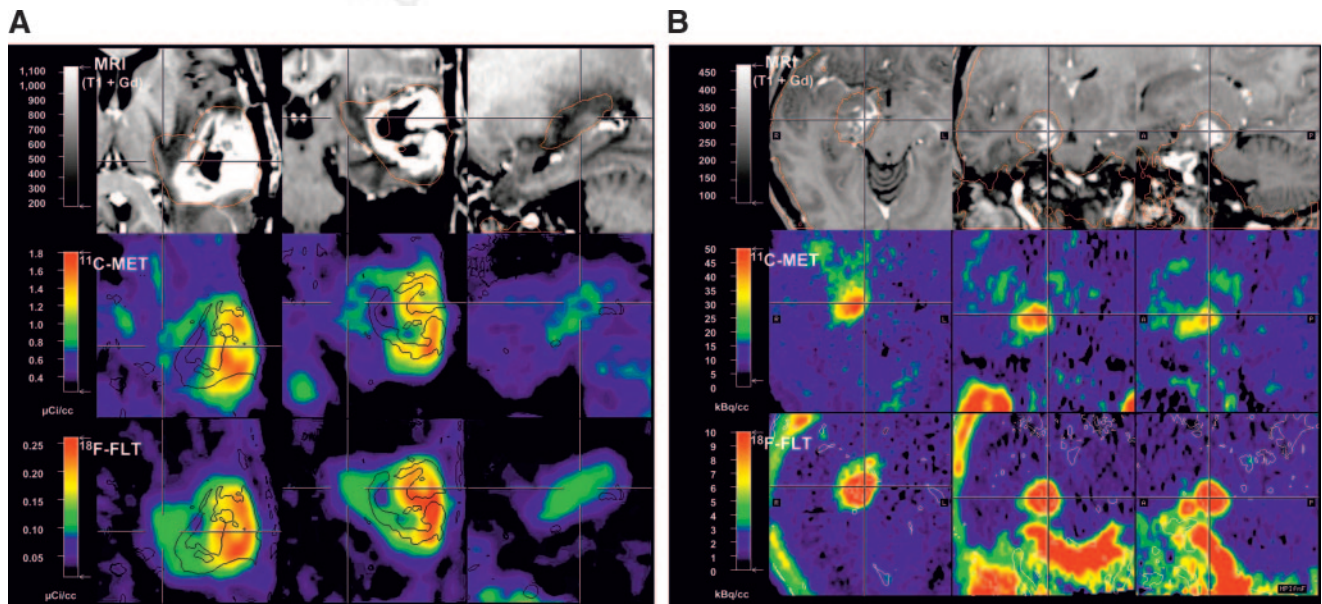
FIGURE 3. Two examples of complementary information on activity and extent of tumor as depicted by multimodal imaging. (A) A 49-y-old woman with recurrent glioblastoma that had been treated by operation, radiation, and 5 cycles of temozolomide. ^{18}F-FLT seems to depict some extension of tumor toward internal capsule and thalamus that was not clearly depicted by gadolinium MRI and ^{11}C-MET PET. Contours on MRI depict tumor extent as measured by ^{18}F-FLT PET; contours on ^{11}C-MET and ^{18}F-FLT PET depict tumor extent as measured by gadolinium enhancement. (B) A 58-y-old woman with WHO grade III ganglioglioma. High tumor activity is depicted by high ^{18}F-FLT uptake (uptake ratio, 13.0; SUV, 3.0), which exceeds involvement shown by gadolinium enhancement to lateral side (volume, 40 cm³ vs. 14.4 cm³). ^{11}C-MET PET shows even further extension of tumor toward pole of temporal lobe. Contours on MRI depict tumor extent as measured by ^{18}F-FLT PET; contours on ^{18}F-FLT PET depict tumor extent as measured by gadolinium enhancement.
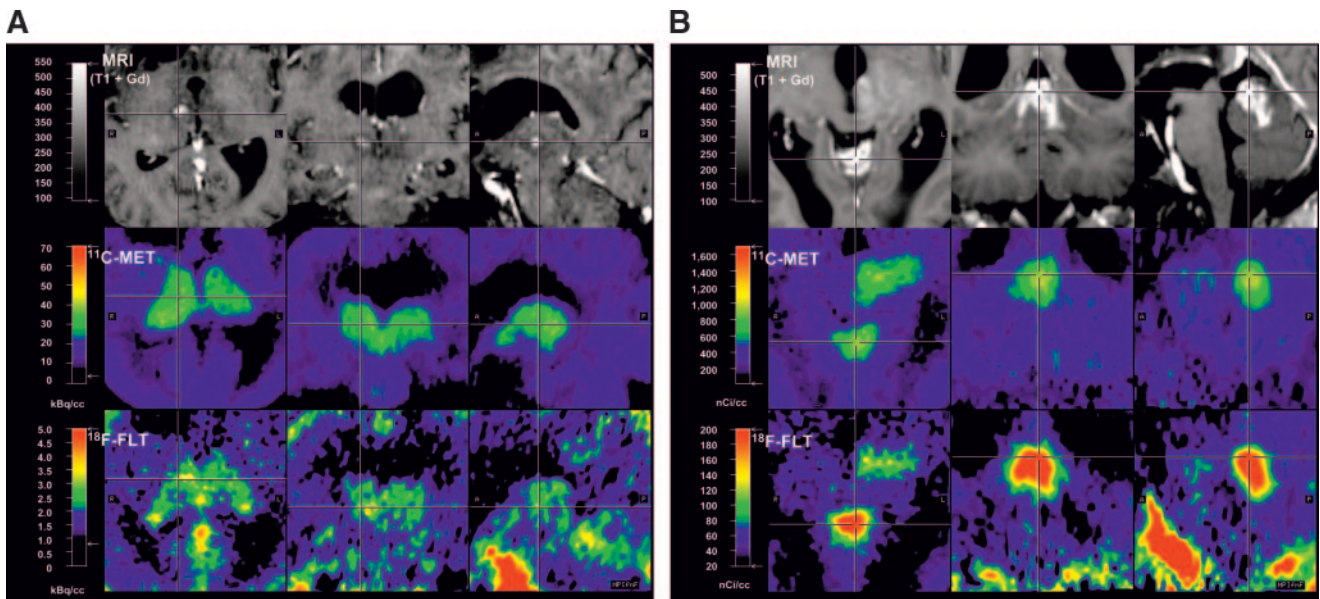
FIGURE 4. Complementary information on tumor activity and extent as depicted by multimodal imaging in 2 patients with tumors near midline. (A) A 57-y-old woman with recurrent WHO grade III oligoastrocytoma in thalamus. Whereas area of gadolinium enhancement is small, ^{11}C-MET and ^{18}F-FLT PET are suggestive of gross involvement of thalami on both sides. (B) A 39-y-old woman with recurrent astrocytoma within vermis and extension into midbrain and thalamus. Gadolinium enhancement is mainly restricted to vermis, whereas ^{11}C-MET and ^{18}F-FLT uptake show clear involvement of left-sided midbrain and thalamus.

These data indicate that both ^{18}F-FLT PET and ^{11}C-MET PET can detect tumor regions that are not detected by gadolinium-enhanced MRI.

For ^{18}F-FLT PET, Uptake Ratio Is Higher and SUVs Are Lower Than Those for ^{11}C-MET PET

Normal cerebral distribution of ^{18}F-FLT is characterized by low background activity in intact brain (Figs. 1 and 2) and significant accumulation within tumor, cranial bone marrow (Figs. 1 and 2), and venous sinuses (Fig. 1B).
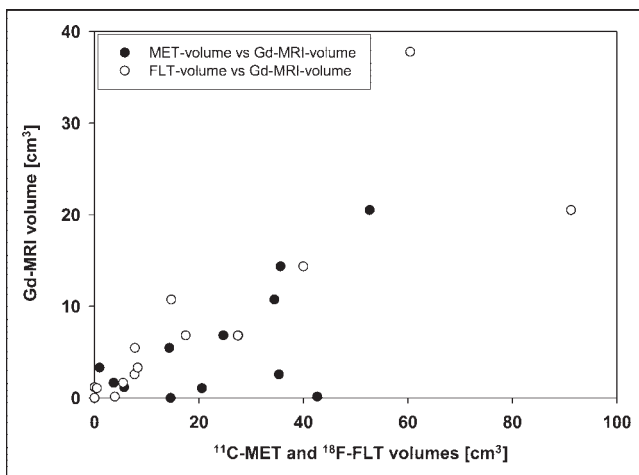

FIGURE 5. Relationship between tumor volumes as measured by gadolinium-enhanced MRI in comparison to ^{11}C-MET PET (●) and ^{18}F-FLT PET (○). In most cases, tumor is larger when measured by PET than when measured by MRI.

Uptake ratios and SUVs were calculated from ROIs placed over the area with maximum tracer uptake, and data are summarized in Table 2. A positive correlation was found between the uptake ratios of ^{11}C-MET and ^{18}F-FLT in the entire patient group (Spearman $r = 0.72$, $P < 0.001$), indicating the relationship between increased uptake and transport rates of amino acids and nucleosides into the tumor. The average uptake ratio of ^{18}F-FLT was significantly higher than the average uptake ratio of ^{11}C-MET in the entire patient group (4.9 ± 3.0 vs. 2.3 ± 0.8, $P < 0.01$ [Wilcoxon]), probably because of the low background activity of ^{18}F-FLT in intact brain relative to tumor tissue. Furthermore, the uptake ratio of ^{18}F-FLT was significantly higher in glioblastomas ($n = 6$) than in astrocytomas ($n = 9$) (6.9 ± 1.9 vs. 3.0 ± 1.4, $P < 0.01$ [Mann–Whitney]). Although no further statistical analysis was performed because of the low numbers in treated and untreated subgroups, these preliminary data already point to a relationship between ^{18}F-FLT uptake and histologic grade and tumor type. The absolute uptake of ^{18}F-FLT was relatively low, with the average SUV for ^{18}F-FLT being significantly lower than the average SUV for ^{11}C-MET (1.3 ± 0.7 vs. 3.1 ± 1.0, $P < 0.01$; Table 2).

Figure 6 gives an overview of average uptake ratios in treated and untreated astrocytoma and glioblastoma patients for ^{18}F-FLT and ^{11}C-MET PET.

Large Parts of Tumors Are Detected by Both ^{18}F-FLT and ^{11}C-MET PET, but Additional Tumor Regions Are Discovered Separately by Each Tracer

For detailed ROI analysis, tumors were segmented into regions with increased tracer uptake of ^{18}F-FLT alone, [11]C-
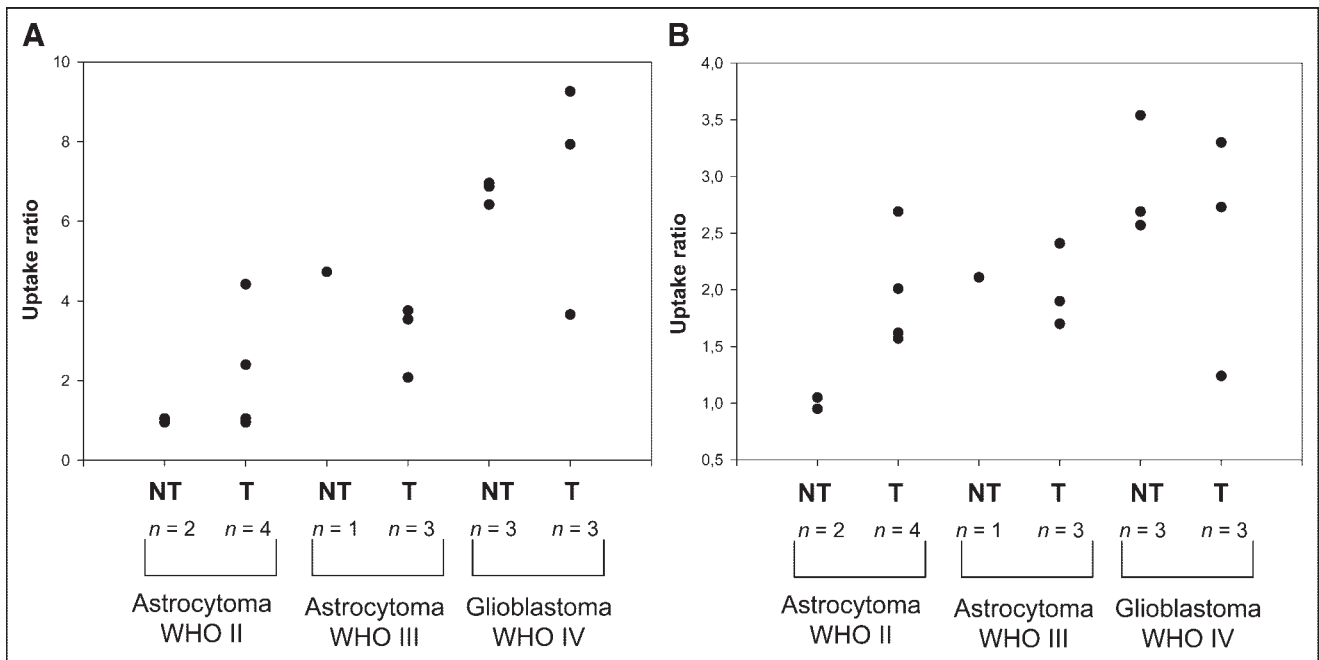
FIGURE 6. Comparison of uptake ratios for ^{18}F-FLT (A) and ^{11}C-MET (B) in treated and untreated astrocytomas and glioblastomas. Uptake ratios of untreated tumors tend to increase with WHO grade. Uptake ratios vary more in treated tumors, most probably because of tissue alterations in response to therapy. NT = no therapy before study inclusion; T = therapy before study inclusion.

MET alone, gadolinium-DTPA alone, or a combination of these using irregularly shaped ROIs. Because of differences in ROI size, the average of the ROIs placed over intact gray and white matter was used as the reference region. For comparison of tumor regions with known highly proliferative tissue, a circular ROI was placed on the nasal mucosa. Uptake ratios for detailed ROIs were then calculated as already described.

High proliferative activity in the nasal mucosa was reflected in a significantly higher uptake ratio for ^{18}F-FLT than for ^{11}C-MET ($P < 0.001$ [Wilcoxon]).

A mean of 2.4 ± 1.0 (range, 1–4) different ROIs were defined in the tumor tissue of 21 patients, and a total of 50 ROIs were evaluated. Regions positive for both PET tracers were identified in most tumors (gadolinium, ^{18}F-FLT, and ^{11}C-MET: $n = 11$; ^{18}F-FLT and ^{11}C-MET: $n = 12$). In these regions, the uptake ratios for ^{18}F-FLT were significantly higher than those for ^{11}C-MET ($P < 0.01$ [Wilcoxon]; gadolinium, ^{18}F-FLT, and ^{11}C-MET: 5.8 ± 3.0 vs. 2.3 ± 0.8; ^{18}F-FLT and ^{11}C-MET: 4.0 ± 2.0 vs. 2.3 ± 0.7). In 13 patients, circumscribed tumor regions were detected by ^{11}C-MET PET only. As expected in these ROIs, uptake ratios for ^{11}C-MET were significantly higher than those for ^{18}F-FLT (2.0 ± 0.4 vs. 1.6 ± 0.4, $P < 0.01$ [Wilcoxon]). In 7 patients, certain tumor regions were positive on ^{18}F-FLT PET only (3.4 ± 1.4 vs. 1.1 ± 0.3, $P < 0.05$ [Wilcoxon]). In the ROIs for gadolinium ($n = 1$) and gadolinium-^{18}F-FLT ($n = 2$), as well as in tumor necrosis ($n = 4$), uptake ratios for ^{18}F-FLT and ^{11}C-MET were not significantly different, most probably because of low sample numbers.

These data indicate that ^{18}F-FLT and ^{11}C-MET detect mainly the same tumor regions, although there are regions detectable only by either ^{18}F-FLT or ^{11}C-MET (Figs. 3 and 4). Furthermore, the presence of regions positive for the respective PET tracer but not showing gadolinium enhancement implies that both ^{18}F-FLT and ^{11}C-MET can detect tumor regions that do not present with gross destruction of the blood–brain barrier as shown by gadolinium-enhanced MRI.

^{18}F-FLT Uptake in Tumor Seems to Be Due to High Transport and Net Influx but Correlates with Phosphorylation Rate by TK$_1$

A representative example of the kinetic analysis is given in Figure 7. ^{18}F-FLT-derived radioactivity in the tumor region peaks in the first 2 min and declines rapidly in the next 5 min, thereafter staying at constant levels (Fig. 7A) that are higher than the radioactivity levels in blood (Fig. 7B) and in the contralateral control region (Fig. 7C). In the kinetic analysis, the 3-compartment model provided a significantly better fit of the data than did the 2-compartment model. Tumor regions were significantly different from the reference region in blood volume, most probably because of higher vascularization of tumor tissue (Tables 3 and 4). Furthermore, Ki and K1 differed significantly, indicative of a higher transport and net influx of ^{18}F-FLT into tumor tissue. Kinetic analysis revealed no significant differences in k3 between tumor and normal brain (Tables 3 and 4). Kinetic analysis including a k4 revealed a significant dif-
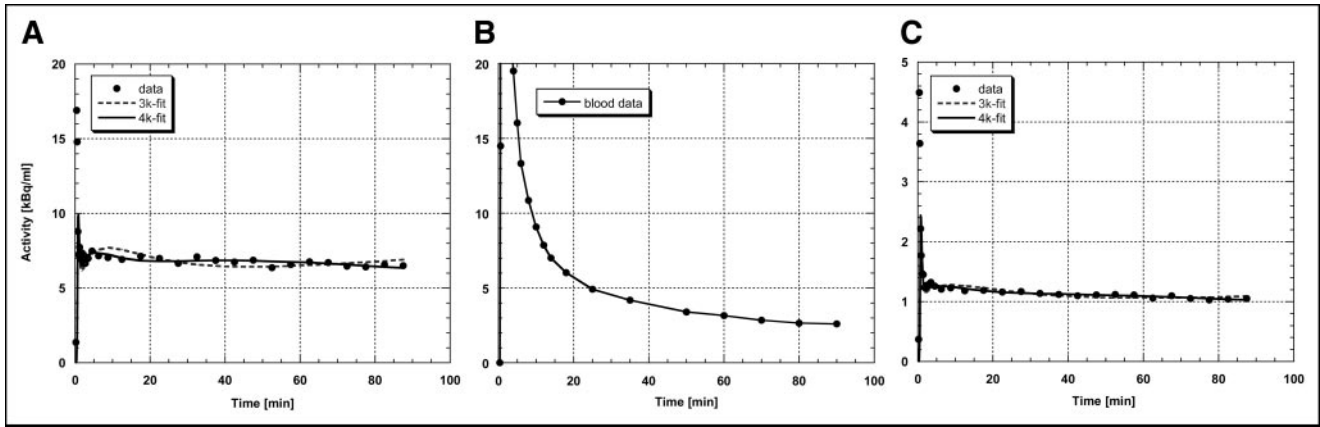
FIGURE 7. Representative measured and fitted time–activity curves from patient 7 (Fig. 1A and Tables 3 and 4). (A) Time–activity curve from tumor region with increased ^{18}F-FLT uptake; simple mean reduced χ^2 value for fit without k4 is 241.1 and with k4 is 250.6. (B) Time–activity curve from blood. (C) Time–activity curve from contralateral control region; simple mean reduced χ^2 value for fit without k4 is 130.3 and with k4 is 134.9. Fifteen minutes or more after radiotracer administration, tumor-to-blood ratio is significantly higher than 1, supporting hypothesis that ^{18}F-FLT uptake is at least partly determined by ^{18}F-FLT trapping and TK1 activity.

ference between tumor and control region, suggesting that a significant amount of ^{18}F-FLT would not be trapped in the tissue (Table 4). There was a good correlation between the net influx (Ki) and the uptake ratio of ^{18}F-FLT in tumor tissue (Spearman $r = 0.88$, $P < 0.001$) and a weaker correlation between the rate constants K1 and k3 and the uptake ratio of ^{18}F-FLT in tumor tissue (K1: Spearman $r = 0.85$, $P < 0.001$; k3: Spearman $r = 0.65$, $P = 0.011$; Fig. 8). Restriction to grade III and IV gliomas ($n = 11$) revealed a stronger correlation between k3 and ^{18}F-FLT uptake ratio (Spearman $r = 0.76$, $P < 0.01$). Multiple-regression anal-

ysis revealed that K1 and k3 are 2 independent factors predicting ^{18}F-FLT uptake (K1: $P < 0.01$; k3: $P < 0.05$). The relationship between K1 and k3 and ^{18}F-FLT uptake is shown in Figure 8. These data point to the relevance of increased transport and net influx of ^{18}F-FLT into tumor tissue but do not exclude the mechanism of increased phosphorylation of ^{18}F-FLT by TK$_1$, as indicated by tumor-to-blood ratios significantly higher than those 15 min and later after tracer application and by the correlation between the uptake ratio for ^{18}F-FLT and the metabolic rate constant k3 in tumor tissue.

TABLE 3
For 14 Patients, Individual Data Obtained by Kinetic Analysis with Fixed k4 of 0

Patient no.	Tumor regions with increased FLT uptake					Contralateral control regions				
	K1	k2	k3	vB	Ki	K1	k2	k3	vB	Ki
2	0.0684	0.0867	0.0210	0.1194	0.0133	0.0093	0.0757	0.0162	0.0213	0.0016
4	0.0928	0.0989	0.0290	0.0831	0.0210	0.0075	0.0500	0.0127	0.0169	0.0015
5	0.0371	0.0398	0.0186	0.0914	0.0118	0.0035	0.0200	0.0024	0.0295	0.0004
7	0.0563	0.0726	0.0189	0.0850	0.0116	0.0076	0.0561	0.0149	0.0216	0.0016
8	0.0338	0.0510	0.0115	0.0821	0.0062	0.0042	0.0405	0.0087	0.0269	0.0007
9	0.0758	0.1176	0.0073	0.1443	0.0044	0.0127	0.0902	0.0106	0.0482	0.0013
10	0.0139	0.0345	0.0040	0.0965	0.0014	0.0046	0.0290	0.0058	0.0516	0.0008
11	0.0198	0.0352	0.0112	0.1364	0.0048	0.0037	0.0205	0.0012	0.0460	0.0002
12	0.0038	0.0131	0.0010	0.0313	0.0003	0.0046	0.0249	0.0040	0.0255	0.0006
13	0.0006	0.0048	0.0000	0.2949	0.0000	0.0033	0.0219	0.0000	0.1456	0.0000
18	0.0113	0.0783	0.0145	0.0229	0.0018	0.0078	0.0796	0.0067	0.0337	0.0006
19	0.0182	0.0403	0.0067	0.0280	0.0026	0.0054	0.0634	0.0114	0.0227	0.0008
20	0.0166	0.0602	0.0152	0.0125	0.0033	0.0069	0.0500	0.0068	0.0169	0.0008
23	0.0380	0.0384	0.0108	0.1435	0.0083	0.0074	0.0436	0.0114	0.0379	0.0015
Mean	0.0347	0.0551	0.0121	0.0980	0.0063	0.0063	0.0475	0.0081	0.0389	0.0009
SD	0.0286	0.0323	0.0081	0.0723	0.0057	0.0027	0.0233	0.0051	0.0328	0.0005
*P**	<0.01	NS	NS	<0.05	<0.01					

*Versus control regions (Mann–Whitney rank sum test).
NS = not statistically significant.

TABLE 4
For 14 Patients, Individual Data Obtained by Kinetic Analysis Including k4

Patient no.	Tumor regions with increased FLT uptake						Contralateral control regions					
	K1	k2	k3	k4	vB	Ki	K1	k2	k3	k4	vB	Ki
2	0.0561	0.2150	0.0955	0.0105	0.1321	0.0173	0.0085	0.2535	0.1294	0.0167	0.0234	0.0029
4	0.1154	0.2622	0.1025	0.0134	0.0764	0.0324	0.0132	0.2312	0.0683	0.0123	0.0149	0.0030
5	0.0381	0.0818	0.0779	0.0179	0.0894	0.0186	0.0036	0.0189	0.0018	0.0000	0.0295	0.0003
7	0.0603	0.1340	0.0656	0.0172	0.0817	0.0198	0.0081	0.0897	0.0486	0.0187	0.0213	0.0028
8	0.0399	0.1097	0.0531	0.0207	0.0477	0.0130	0.0227	0.0694	0.0274	0.0104	0.0459	0.0064
9	0.0653	0.1030	0.0072	0.0024	0.1440	0.0043	0.0140	0.1406	0.0395	0.0236	0.0471	0.0031
10	0.0124	0.0492	0.3539	0.4032	0.0968	0.0109	0.0043	0.0243	0.0031	0.0000	0.0517	0.0005
11	0.0558	0.3400	0.0990	0.0196	0.0915	0.0126	0.0035	0.0186	0.0002	0.0000	0.0461	0.0000
12	0.0082	0.0144	0.0012	0.0003	0.0373	0.0007	0.0046	0.0250	0.0043	0.0000	0.0255	0.0007
13	0.1061	0.3949	0.0023	0.0246	0.0400	0.0006	0.0029	0.0191	0.0000	0.0000	0.1456	0.0000
18	0.0117	0.0939	0.0250	0.0097	0.0225	0.0025	0.0177	0.6604	0.0872	0.0130	0.0291	0.0021
19	0.0186	0.0530	0.0266	0.0275	0.0276	0.0062	0.0057	0.0882	0.0334	0.0193	0.0225	0.0016
20	0.0179	0.0943	0.0474	0.0184	0.0119	0.0060	0.0069	0.0500	0.0067	0.0000	0.0168	0.0008
23	0.0411	0.0924	0.0704	0.0235	0.1369	0.0178	0.0075	0.0537	0.0243	0.0138	0.0376	0.0023
Mean	0.0462	0.1456	0.0734	0.0435	0.0740	0.0116	0.0088	0.1245	0.0339	0.0091	0.0398	0.0019
SD	0.0335	0.1140	0.0882	0.1038	0.0440	0.0090	0.0060	0.1721	0.0386	0.0088	0.0328	0.0017
P*	<0.01	NS	NS	<0.05	<0.05	<0.01						

*Versus control regions (Mann–Whitney rank sum test).
NS = not statistically significant.

Tables 3 and 4 give the individual data of the kinetic analysis obtained from the tumor and reference regions of 14 patients with and without inclusion of k4.

DISCUSSION

To our knowledge, this is the first clinical study to include kinetic modeling in a systematic comparison of ^{18}F-FLT PET with ^{11}C-MET PET in human gliomas. We demonstrate, first, that absolute uptake of ^{18}F-FLT is lower than that of ^{11}C-MET (SUV, 1.3 ± 0.7 vs. 3.1 ± 1.0) and that the uptake ratios for tumor to normal brain are higher (4.9 ± 3.0 vs. 2.3 ± 0.8) because of the low uptake of ^{18}F-FLT in

FIGURE 8. Correlation of K1 and k3 with ^{18}F-FLT uptake ratio. Spearman rank correlation coefficients are $r = 0.85$ for K1 ($P < 0.001$) and $r = 0.65$ for k3 ($P = 0.011$).

normal brain; second, that sensitivity for the detection of tumor is lower for ^{18}F-FLT than for ^{11}C-MET (78.3% vs. 91.3%), especially in low-grade gliomas; third, that in individual patients, ^{18}F-FLT, ^{11}C-MET PET, and gadolinium-enhanced MRI give complementary information on the true extent of the tumor; fourth, that ^{18}F-FLT is taken up predominantly in tumor regions with a disrupted blood–brain barrier; and fifth, that a variable combination of different processes, such as increased transport and phosphorylation and blood–brain barrier disruption, leads to ^{18}F-FLT accumulation.

For the management of malignant gliomas, it is of the utmost importance to detect those areas where the tumor progresses into the neighboring tissue, because recurrence of the tumor—and the fate of the patient—highly depends on the extent and activity of this proliferation zone. This area should therefore be the main target of invasive diagnostic and therapeutic strategies. Often, these regions cannot be clearly distinguished from edema or necrosis by morphologic imaging modalities such as CT or MRI, and they may escape detection by ^{18}F-FDG PET because of the high-energy metabolism of normal gray matter obscuring subtle increases of ^{18}F-FDG uptake in tumorous tissue with low cellular density (22). ^{11}C-MET therefore has been introduced to better delineate the extent of gliomas because its selective transport into tumorous tissue results in a high contrast to normal brain where uptake of this tracer is low. However, the short half-life of this tracer does not permit evaluation of protein synthesis, and therefore, the increased uptake is probably related more to microvessel density (5) than to cellular proliferation. Labeled nucleotides, such as
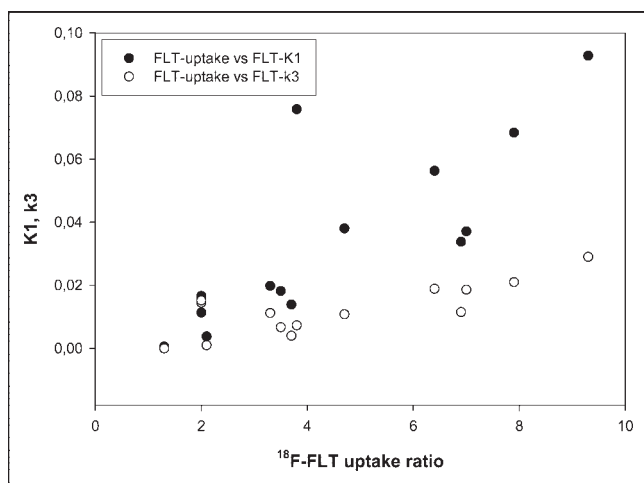
tritiated thymidine, have been widely used in experimental models to quantitate tumor DNA synthesis (23). Moreover, ^{11}C-thymidine was shown to be especially useful as an imaging agent for determining tumor proliferation (24), but the short half-life and the necessary complex analysis of data due to large amounts of labeled molecules limited the application of this tracer in the clinical workup of patients with brain tumors. With ^{18}F-FLT, a tracer was introduced (6) that has a half-life well suited for clinical application. Additionally, trapping of the product phosphorylated by thymidine kinase, the target enzyme, permits the analysis of accumulation kinetics in a 3-compartment model. The high correlation to thymidine uptake suggests that ^{18}F-FLT accumulation is a reliable measure of the salvage pathway of DNA synthesis (15,25). As a consequence, this compound has found many applications in oncology (26) and, despite some limitations, is widely accepted as a marker for tumor cell proliferation. However, despite the advantage of a low uptake of ^{18}F-FLT in normal brain, only a few studies on brain tumors have been reported.

The most detailed analysis so far was one recently reported on 25 patients with newly diagnosed ($n = 7$) or previously treated ($n = 18$) glioma. The study used ^{18}F-FLT and ^{18}F-FDG PET, as well as Ki-67 staining in a subgroup of patients (27). This study showed a rapid ^{18}F-FLT uptake, peaking at 5–10 min after application and remaining stable up to 75 min; excellent delineation of WHO grades III and IV tumors, with low absolute uptake (mean SUV, 1.33) but excellent image contrast (tumor-to-normal ratio, 3.85); no appreciable ^{18}F-FLT uptake in WHO grade II gliomas and stable lesions; and a high correlation of ^{18}F-FLT SUV with Ki-67 expression as an indication that ^{18}F-FLT is a surrogate marker for tumor proliferation in high-grade gliomas (27). Our results are in accordance with the findings of Chen et al. (27) with regard to low SUV, low uptake in normal brain, and resulting high tumor-to-normal ratios. Moreover, our study, in being the first to compare ^{18}F-FLT uptake with ^{11}C-MET uptake, apply kinetic analysis to the 3-compartment model of ^{18}F-FLT uptake in a larger group of patients with various gliomas, and differentiate between transport and increased tracer retention associated with tumor proliferation, extends these findings. Our results also extend previous findings with 2-^{11}C-thymidine applying sequential ^{11}C-CO$_2$ and ^{11}C-thymidine scans and analysis of filtered data in a 5-compartment model (24,28). Two types of tissue compartments could be identified by the 3 imaging parameters: tissue compartments with elevated gadolinium enhancement, elevated ^{11}C-MET uptake, and elevated ^{18}F-FLT uptake (here, disruption of the blood–brain barrier is the most likely cause of ^{11}C-MET and ^{18}F-FLT uptake) and tissue compartments with positive ^{11}C-MET and ^{18}F-FLT uptake and without obvious disruption of the blood–brain barrier, at least not as depicted by gadolinium-enhanced MRI (here, ^{18}F-FLT and ^{11}C-MET uptake is most likely due to increased transport of nucleosides and amino acids into the tumor). The facts that k2 is not significantly different between tumor and control regions and that k3 correlates with FLT uptake suggests that phosphorylation and trapping also play a role in ^{18}F-FLT uptake. In summary, the regional distribution of ^{18}F-FLT uptake with and without positive contrast enhancement on MRI and with and without accumulation of ^{11}C-MET suggests the presence of various tissue compartments in which ^{18}F-FLT accumulation is due to the breakdown of the blood–brain barrier, increased transport, increased proliferation, or a variable combination of these components.

In all positive tumors, the gadolinium-enhanced volumes on MRI were smaller than the volumes with significantly increased accumulation of ^{18}F-FLT or ^{11}C-MET, indicating an increased transport of these tracers into active tumorous tissue even before the blood–brain barrier breaks down substantially. Because the transport characteristics of fluorinated nucleosides would not lead one to expect a substantial uptake without a disrupted blood–brain barrier, our findings might also suggest ^{18}F-FLT as the more sensitive marker for blood–brain barrier disruption, and it may well be that subtle blood–brain barrier leakage is not depicted as gadolinium enhancement and 3-dimensional volumetry. Nevertheless, for both tracers a correlation between the increased transport and the proliferation rate has been demonstrated (2–4,6,28). Because k3 showed no statistically significant difference between tumor and control region, our data do not permit the clear conclusion that ^{18}F-FLT accumulates significantly in gliomas as a consequence of phosphorylation and irreversible trapping in proliferating cells. With k3 values significantly greater than zero in the control region, our data may even suggest Ki as the more robust parameter, in which case the normal brain is very low. However, because we observed a significant correlation between the uptake ratio of ^{18}F-FLT and the metabolic rate constants K1 and k3 (Fig. 8), these data indicate that FLT uptake is due to a combination of factors, including increased transport and phosphorylation. Including a k4 in our analysis minimally altered the goodness of fit (Fig. 7), but whether k4 plays a substantial role is unresolved and deserves further investigation.

In some tumor regions, ^{18}F-FLT does not accumulate despite increased uptake of ^{11}C-MET. This discrepancy might be due to the selectivity of thymidine kinase as the target of ^{18}F-FLT for the salvage pathway of DNA synthesis (15,25,29). In tumor cell lines using de novo DNA synthesis, the proliferation rate might be underestimated by this tracer (30). The fact that this patient population was heterogeneous, with 9 of 23 patients pretreated by radiation therapy, might have had some influence on the state of the blood–brain barrier with subsequent alteration of ^{18}F-FLT uptake.

CONCLUSION

This study demonstrated that ^{18}F-FLT is a promising tracer for the detection and characterization of brain tumors.

Compared with ^{18}F-FDG, ^{18}F-FLT has the advantage of high uptake in tumors in relation to the low background in normal brain tissue. Compared with ^{11}C-MET, the longer half-life of ^{18}F-FLT permits the follow-up of increased transport into tumor cells. Our preliminary data in a relatively small and heterogeneous patient population do not support the clear conclusion that analysis of glioma cell proliferation, which is the target for evaluation of early treatment effects in humans, is possible. However, the study indicated that ^{18}F-FLT uptake differentiates low-grade from high-grade gliomas; that ^{18}F-FLT uptake is due to a combination of factors, including increased transport and phosphorylation; and that ^{18}F-FLT PET might provide information on the extent and activity of a glioma additional to that provided by MRI and ^{11}C-MET. Further studies might find feasible the determination of typical signatures of various brain tumors and the assessment of the value of ^{18}F-FLT as a tracer for early evaluation of treatment effects in patients with gliomas.

REFERENCES

1. Jacobs AH, Dittmar C, Winkeler A, Garlip G, Heiss WD. Molecular imaging of gliomas. *Mol Imaging.* 2002;1:309–335.
2. Chung JK, Kim YK, Kim SK, et al. Usefulness of ^{11}C-methionine PET in the evaluation of brain lesions that are hypo- or isometabolic on ^{18}F-FDG PET. *Eur J Nucl Med Mol Imaging.* 2002;29:176–182.
3. Langen KJ, Muhlensiepen H, Holschbach M, Hautzel H, Jansen P, Coenen HH. Transport mechanisms of 3-[^{123}I]iodo-alpha-methyl-L-tyrosine in a human glioma cell line: comparison with [^{3}H]methyl]-L-methionine. *J Nucl Med.* 2000;41:1250–1255.
4. Sato N, Suzuki M, Kuwata N, et al. Evaluation of the malignancy of glioma using ^{11}C-methionine positron emission tomography and proliferating cell nuclear antigen staining. *Neurosurg Rev.* 1999;22:210–214.
5. Kracht LW, Friese M, Herholz K, et al. Methyl-[^{11}C]-l-methionine uptake as measured by positron emission tomography correlates to microvessel density in patients with glioma. *Eur J Nucl Med Mol Imaging.* 2003;30:868–873.
6. Shields AF, Grierson JR, Dohmen BM, et al. Imaging proliferation in vivo with [F-18]FLT and positron emission tomography. *Nat Med.* 1998;4:1334–1336.
7. Kong XB, Zhu QY, Vidal PM, et al. Comparisons of anti-human immunodeficiency virus activities, cellular transport, and plasma and intracellular pharmacokinetics of 3'-fluoro-3'-deoxythymidine and 3'-azido-3'-deoxythymidine. *Antimicrob Agents Chemother.* 1992;36:808–818.
8. Sherley JL, Kelly TJ. Regulation of human thymidine kinase during the cell cycle. *J Biol Chem.* 1988;263:8350–8358.
9. Hengstschlager M, Knofler M, Mullner EW, Ogris E, Wintersberger E, Wawra E. Different regulation of thymidine kinase during the cell cycle of normal versus DNA tumor virus-transformed cells. *J Biol Chem.* 1994;269:13836–13842.
10. Toyohara J, Waki A, Takamatsu S, Yonekura Y, Magata Y, Fujibayashi Y. Basis of FLT as a cell proliferation marker: comparative uptake studies with [^{3}H]thymidine and [^{3}H]arabinothymidine, and cell-analysis in 22 asynchronously growing tumor cell lines. *Nucl Med Biol.* 2002;29:281–287.
11. Buck AK, Schirrmeister H, Hetzel M, et al. 3-deoxy-3-[(18)F]fluorothymidine-positron emission tomography for noninvasive assessment of proliferation in pulmonary nodules. *Cancer Res.* 2002;62:3331–3334.
12. Cobben DC, Jager PL, Elsinga PH, Maas B, Suurmeijer AJ, Hoekstra HJ. 3'-^{18}F-fluoro-3'-deoxy-L-thymidine: a new tracer for staging metastatic melanoma? *J Nucl Med.* 2003;44:1927–1932.
13. Francis DL, Visvikis D, Costa DC, et al. Potential impact of [^{18}F]3'-deoxy-3'-fluorothymidine versus [^{18}F]fluoro-2-deoxy-D-glucose in positron emission tomography for colorectal cancer. *Eur J Nucl Med Mol Imaging.* 2003;30:988–994.
14. Wagner M, Seitz U, Buck A, et al. 3'-[^{18}F]fluoro-3'-deoxythymidine ([^{18}F]-FLT) as positron emission tomography tracer for imaging proliferation in a murine B-cell lymphoma model and in the human disease. *Cancer Res.* 2003;632681–2687.
15. Rasey JS, Grierson JR, Wiens LW, Kolb PD, Schwartz JL. Validation of FLT uptake as a measure of thymidine kinase-1 activity in A549 carcinoma cells. *J Nucl Med.* 2002;43:1210–1217.
16. Machulla HJ, Blocher A, Kuntzsch M, Piert M, Wei R, Grierson JR. Simplified labeling approach for synthesizing 3'-deoxy-3'-[^{18}F]fluorothymidine ([^{18}F]FLT). *J Radioanal Nucl Chem.* 2000;243:843–846.
17. Wodarski C, Eisenbarth J, Weber K, Henze M, Haberkorn U, Eisenhut M. Synthesis of 3'-deoxy-3'-[^{18}F]fluoro-thymidine with 2,3'-anhydro-5'-O-(4,4'-dimethoxytrityl)-thymidine. *J Labelled Compds Radiopharm.* 2000;43:1211–1218.
18. Kracht LW, Miletic H, Busch S, et al. Delineation of brain tumor extent with [^{11}C]L-methionine positron emission tomography: local comparison with stereotactic histopathology. *Clin Cancer Res.* 2004;10:7163–7170.
19. Herholz K, Holzer T, Bauer B, et al. ^{11}C-Methionine PET for differential diagnosis of low-grade gliomas. *Neurology.* 1998;50:1316–1322.
20. Shields AF, Grierson JR, Muzik O, et al. Kinetics of 3'-deoxy-3'-[F-18]fluorothymidine uptake and retention in dogs. *Mol Imaging Biol.* 2002;4:83–89.
21. Visvikis D, Francis D, Mulligan R, et al. Comparison of methodologies for the in vivo assessment of [18]FLT utilisation in colorectal cancer. *Eur J Nucl Med Mol Imaging.* 2004;31:169–178.
22. Herholz K, Pietrzyk U, Voges J, et al. Correlation of glucose consumption and tumor cell density in astrocytomas: a stereotactic PET study. *J Neurosurg.* 1993;79:853–858.
23. Livingston RB, Hart JS. The clinical applications of cell kinetics in cancer therapy. *Annu Rev Pharmacol Toxicol.* 1977;17:529–543.
24. Eary JF, Mankoff DA, Spence AM, et al. 2-[C-11]thymidine imaging of malignant brain tumors. *Cancer Res.* 1999;59:615–621.
25. Schwartz JL, Tamura Y, Jordan R, Grierson JR, Krohn KA. Monitoring tumor cell proliferation by targeting DNA synthetic processes with thymidine and thymidine analogs. *J Nucl Med.* 2003;44:2027–2032.
26. Been LB, Suurmeijer AJ, Cobben DC, Jager PL, Hoekstra HJ, Elsinga PH. [(18)F]FLT-PET in oncology: current status and opportunities. *Eur J Nucl Med Mol Imaging.* 2004;31:1659–1672.
27. Chen W, Cloughesy T, Kamdar N, et al. Imaging proliferation in brain tumors with ^{18}F-FLT PET: comparison with ^{18}F-FDG. *J Nucl Med.* 2005;46:945–952.
28. Wells JM, Mankoff DA, Eary JF, et al. Kinetic analysis of 2-[^{11}C]thymidine PET imaging studies of malignant brain tumors: preliminary patient results. *Mol Imaging.* 2002;1:145–150.
29. Dittmann H, Dohmen BM, Kehlbach R, et al. Early changes in [^{18}F]FLT uptake after chemotherapy: an experimental study. *Eur J Nucl Med Mol Imaging.* 2002;29:1462–1469.
30. Spyratos F, Ferrero-Pous M, Trassard M, et al. Correlation between MIB-1 and other proliferation markers: clinical implications of the MIB-1 cutoff value. *Cancer.* 2002;94:2151–2159.